Adaptive Control of Multi-Agent Systems for Finding Peaks of Uncertain Static Fields

Mahdi Jadaliha, Joonho Lee,* and Jongeun Choi†

Abstract

In this paper, we design and analyze a class of multi-agent systems that locate peaks of uncertain static fields in a distributed and scalable manner. Our approach builds on adaptive control. The scalar field of interest is assumed to be generated by a radial basis network function. Each agent is driven by swarming and gradient ascent efforts based on its own recursively estimated field via locally collected measurements by itself and its neighboring agents. The convergence properties of the proposed multi-agent systems are analyzed. We also propose a sampling scheme to facilitate the convergence. We provide simulation results by applying our proposed algorithms to fully actuated nonholonomic differentially driven mobile robots under different conditions. The extensive simulation results match well with the predicted behaviors from the convergence analysis, and illustrate the usefulness of the proposed coordination and sampling algorithms.

Keywords: Mobile Sensing Networks, Cooperative Control, Adaptive Control

*Mahdi Jadaliha and Joonho Lee are with the Departments of the Mechanical Engineering, Michigan State University.

†Jongeun Choi (corresponding author) is with the Departments of the Mechanical Engineering and Electrical and Computer Engineering, Michigan State University, East Lansing, MI 48824-1226, U.S.A. Email: jchoi@egr.msu.edu

1 Introduction

In recent years, due to significant progress in sensing, communication, and embedded-system technologies, many research activities have been focused on the areas of mobile sensor networks and multi-agent systems [1, 2, 3, 4]. Mobile sensor networks usually form an ad-hoc wireless communication network in which each agent shares information with neighboring agents within a short communication range, with limited memory and computational power. Although each agent has limited capabilities, as a group, the multi-agent system may perform various tasks at a level which is compatible to a small number of high-end mobile agents. In order to achieve a global goal such as exploration, surveillance, and environmental monitoring, mobile sensing agents require distributed coordination to deal with uncertain environments.

Decentralized and adaptive control algorithms have been proposed in [4] for networks of robots to converge to optimal sensing configurations while simultaneously learning the distribution of sensory information in the environment.

Tanner [5] and Olfati-Saber [2] developed comprehensive analyses of the flocking algorithm by Reynolds [6]. In general, the collective swarm behaviors of birds and fish are known to be the outcomes of natural optimization [7, 8]. These flocking algorithms have been used to move mobile sensor networks in groups [9].

Among other problems in mobile sensor networks, finding peaks of a scalar field of interest has attracted much attention of control engineers [10, 11, 12, 9]. This is due to numerous applications of tracking toxins by robotic sensors in uncertain environments. Such demand exists in environmental monitoring where a dominant method for monitoring of environmental variables (e.g., biomass of harmful algal blooms) is still manual sampling followed by lab analysis. For example, each robotic sensor may carry sensors for sampling pH, blue-green algae (cyanobacteria), Chlorophyll *a* (total biomass of algae/phytoplankton) and dissolved oxygen to investigate the growth of harmful algal blooms in fresh water. The detrimental effects of harmful environmental variables can be seen from satellite images in a large scale with a low resolution. For example, Figs. 1(a) and (b) show the dead zone created by harmful algal blooms and the oil slick in the Gulf of Mexico, respectively.

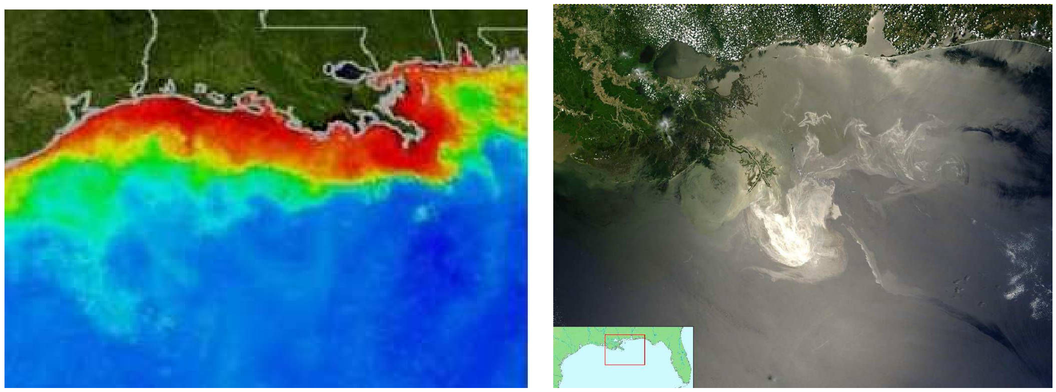

(a) (b)

Figure 1: (a) Dead zone created by algal blooms in the Gulf of Mexico (NASA). (b) The oil slick as seen from space by NASA's Terra satellite on May 24, 2010 (Photo courtesy of NASA).

The cooperative network of agents that performs adaptive gradient climbing in a distributed environment was presented in [10, 11]. The centralized network can adapt its configuration in response to the sensed environment in order to optimize its gradient climb.

In [9], distributed learning and control algorithms are proposed to be executed by each agent independently to estimate a scalar field of interest from noisy measurements and to coordinate multiple agents in a distributed manner to discover peaks of the field. Each mobile agent moves towards peaks of the field using the gradient of its estimated field while avoiding collision and maintaining communication connectivity. The convergence properties of the resulting collective stochastic algorithm were analyzed using the Ljung's ODE approach. In the analysis, the estimation error dynamics have been averaged out under sufficient conditions and so only the ODE of the controlled multi-agent system dynamics could be considered.

In this paper, we design and analyze a class of multi-agent systems that locate peaks of static scalar fields in a distributed and scalable manner. Our approach builds on adaptive control. The scalar field of interest is assumed to be generated by a radial basis network function. We use the flocking algorithm for robotic sensors to make spatially distributed sampling and to maintain communication connectivity. The proposed distributed adaptive control consists of the swarming effort and the gradient ascent motion control based on the recursively estimated field. The associated recursive estimation laws have been developed by gradient-based and recursive least squares

(RLS) algorithms. In contrast to [9], the closed-loop dynamics combining the motion control of the multi-agent system and the parameter estimation error dynamics under proposed strategies have been analyzed. A set of sufficient conditions for which the convergence of the closed-loop multi-agent system is achieved has been provided. To facilitate the successful convergence, we provide an additional scalable and distributed sampling strategy that keeps selective past measurements. We also provide simulation results by applying our proposed algorithms to fully actuated nonholonomic differentially driven mobile robots under different conditions. The extensive simulation study illustrates the effectiveness of the proposed schemes.

The remainder of this paper is organized as follows. Models for the resource-constrained multi-agent systems and the static environmental field are introduced in Sections 2 and 3, respectively. From the models and the motivations, the problem of synthesizing and analyzing coordination algorithms is formulated in Section 4. The proposed distributed adaptive control for multi-agent systems is proposed in Section 5. The main result on the convergence properties of the closed-loop multi-agent systems under the proposed control strategies is provided in Section 5.4. Simulation results are given in Section 7 demonstrating the usefulness of the proposed schemes.

Standard notation will be used throughout the paper. Let $\mathbb{R}, \mathbb{R}_{\geq 0}, \mathbb{R}_{>0}$ denote, respectively, the set of real, non-negative real, and positive real. The positive definiteness (respectively, semi-definiteness) of a matrix A is denoted by $A \succ 0$ (respectively, $A \succeq 0$). $I_n \in \mathbb{R}^{n\times n}$ denotes the identity matrix of size n. $\mathbf{1}_n \in \mathbb{R}^n$ denotes the column vector of size n whose elements are 1. $|N|$ denotes the cardinality of the set N. For column vectors $v_a \in \mathbb{R}^a$, $v_b \in \mathbb{R}^b$, and $v_c \in \mathbb{R}^c$, col$(v_a, v_b, v_c) := \begin{bmatrix} v_a^T & v_b^T & v_c^T \end{bmatrix}^T \in \mathbb{R}^{a+b+c}$ stacks all vectors to create one column vector. $\|v\|$ denotes the Euclidean norm (or the vector 2-norm) of a vector $v \in \mathbb{R}^n$. diag(A, B) denotes the (generalized) block diagonal matrix of $A \in \mathbb{R}^{a\times m}$, $B \in \mathbb{R}^{b\times n}$ and is defined by diag$(A, B) = \begin{bmatrix} A & 0 \\ 0 & B \end{bmatrix} \in \mathbb{R}^{(a+b)\times(m+n)}$. Other notation will be explained in due course.

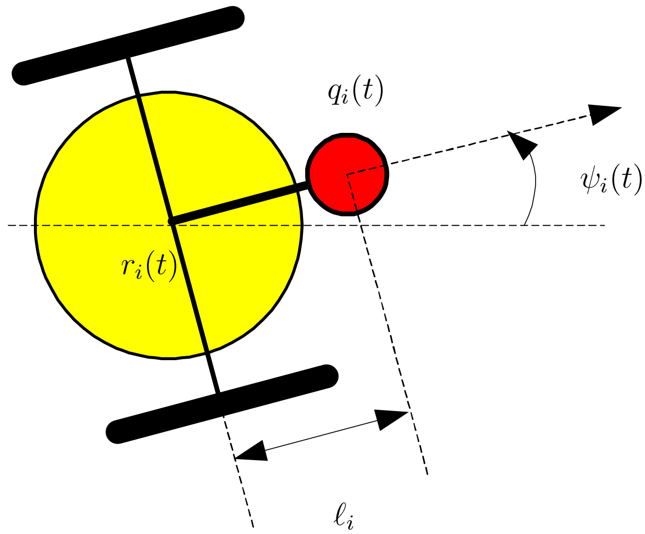

Figure 2: The position of the sensor and states of robot i.

2 Multi-agent systems

In this section, we describe the resource-constrained multi-agent system regarding its individual dynamics and limited communication capability in Sections 2.1 and 2.2, respectively.

2.1 Individual dynamics

We assume that n sensing agents are distributed over the surveillance region $Q \subset \mathbb{R}^2$. Q is assumed to be a convex and compact set. The identity of each agent is indexed by $\mathcal{I} := \{1, 2, \cdots, n\}$. Let $q_i(t) \in Q$ be the location of the sensor attached to agent i at time $t \in \mathbb{R}_{\geq 0}$. Let $q := \mathrm{col}(q_1, q_2, \cdots, q_n) \in \mathbb{R}^{2n}$ be the configuration of the multi-agent system.

Consider a collection of multiple agents, each of which is a nonholonomic differentially driven mobile agent as shown in Fig. 2. In this case, the equations of motion for mobile agent i [13, 14]

may be given by

$$\begin{bmatrix} \dot{r}_{xi}(t) \\ \dot{r}_{yi}(t) \\ \dot{\psi}_i(t) \\ \dot{v}_i(t) \\ \dot{\omega}_i(t) \end{bmatrix} = \begin{bmatrix} v_i \cos\psi_i(t) \\ v_i \sin\psi_i(t) \\ \omega_i(t) \\ 0 \\ 0 \end{bmatrix} + \begin{bmatrix} 0 & 0 \\ 0 & 0 \\ 0 & 0 \\ \frac{1}{m_i} & 0 \\ 0 & \frac{1}{J_i} \end{bmatrix} \begin{bmatrix} F_i(t) \\ \tau_i(t) \end{bmatrix}, \tag{1}$$

where $r_i = [r_{xi},\ r_{yi}]^T$ and ψ_i denote the inertial position and the orientation of agent i, respectively. v_i and ω_i are linear and angular speeds, respectively. F_i and τ_i denote force and torque inputs. m_i and J_i are the mass and the moment of inertia. In this paper, we need to control the sensor location. Let the sensor location be at a point that is on a center line perpendicular to the wheel axis and is ℓ_i distance away from the wheel axis, i.e., $\|q_i(t) - r_i(t)\| = \ell_i$ as shown in Fig. 2. The sensor location can be described by

$$q_i(t) = r_i(t) + \ell_i \begin{bmatrix} \cos\psi_i(t) \\ \sin\psi_i(t) \end{bmatrix}. \tag{2}$$

By differentiating $q_i(t)$ twice with respect to time t, we obtain

$$\begin{aligned} \ddot{q}_i(t) = & \begin{bmatrix} -v_i(t)\omega_i(t)\sin\psi_i(t) - \ell_i\omega_i^2(t)\cos\psi_i(t) \\ v_i(t)\omega_i(t)\cos\psi_i(t) - \ell_i\omega_i^2(t)\sin\psi_i(t) \end{bmatrix} \\ & + \begin{bmatrix} \frac{1}{m_i}\cos\psi_i(t) & -\frac{\ell_i}{J_i}\sin\psi_i(t) \\ \frac{1}{m_i}\sin\psi_i(t) & \frac{\ell_i}{J_i}\cos\psi_i(t) \end{bmatrix} \begin{bmatrix} F_i(t) \\ \tau_i(t) \end{bmatrix} \\ =: & \ A(t) + B(t) \begin{bmatrix} F_i(t) \\ \tau_i(t) \end{bmatrix}. \end{aligned} \tag{3}$$

Since $B(t)$ is nonsingular as long as $\|q_i(t) - r_i(t)\| = \ell_i \neq 0$, we can perform the output feedback linearization at the sensor location $q_i(t)$ using the output feedback linearizing control [13] given as follows.

$$\begin{bmatrix} F_i(t) \\ \tau_i(t) \end{bmatrix} = B^{-1}(t) \times (u_i(t) - A(t)). \tag{4}$$

With this feedback linearizing control in (4) being applied to (3), we obtain that $\ddot{q}_i(t) = u_i(t)$. It can be shown that the zero dynamics are stable [13] and differentiating (2) shows that $\omega_i(t) \to 0$ and $v_i(t) \to 0$ as $\dot{q}_i(t) \to 0$.

There exists a large class of holonomic vehicle models with some conditions [15, 16] that can be output feedback linearized with respect to the sensor location to obtain the similar result. It is shown that a dynamic model of a holonomic mobile robot with four-powered wheels can be linearized and decoupled [17].

Therefore, without loss of generality, we assume that the dynamics of sensing agent i (its sensor location) is given by

$$\begin{aligned} \dot{q}_i(t) &= p_i(t), \\ \dot{p}_i(t) &= u_i(t), \end{aligned} \tag{5}$$

where $p_i(t)$ is the velocity of agent i and $u_i(t)$ is the input of agent i. For the case of the non-holonomic model described in (1), the proposed control $u_i(t)$ in this paper can be implemented by $F_i(t)$ and $\tau_i(t)$, which are obtained by plugging $u_i(t)$ in (4).

2.2 Limited communication capability

We use the graph notation in order to describe the group behavior of the multi-agent system based on the limited communication capability of each agent. We assume that each agent can communicate with its neighboring agents within a limited transmission range, which is given by a radius of r. The neighborhood of agent i with a configuration of q is defined by $\mathcal{N}(i,q) := \{j \in \mathcal{I} \mid (i,j) \in \mathcal{E}(q)\}$. Therefore, $(i,j) \in \mathcal{E}(q)$ if and only if $\|q_i(t) - q_j(t)\| \leq r$. We often use $\mathcal{N}_i$ instead of using $\mathcal{N}(i,q)$ for notational simplicity. We define $\overline{\mathcal{N}}_i$ as the union of index i and indices of its neighbors, i.e., $\overline{\mathcal{N}}_i := \{i\} \cup \mathcal{N}_i$. We use the adjacency matrix $A := [a_{ij}]$ of an undirected graph G as defined in [1]. $A := [a_{ij}]$ is symmetrical. The element a_{ij} of adjacency matrix is defined as $a_{ij} = \sigma_w(\epsilon - d_{ij})$, with $\sigma_w(y) = \frac{1}{1+e^{-wy}}$, where d_{ij} is a distance between neighboring agent j and agent i itself, σ_w is the sigmoid function with constants $w > 0$ and $\epsilon > 0$. The scalar graph Laplacian $L = [l_{ij}] \in \mathbb{R}^{n \times n}$ is a matrix defined as $L := D(A) - A$, where $D(A)$ is a diagonal matrix given by, i.e., $D(A) := \text{diag}(\sum_{j=1}^{n} a_{ij})$. The 2-dimensional graph Laplacian is defined as $\hat{L}_2 := L \otimes I_2$, where $\otimes$ is the Kronecker product.

3 Static scalar environmental field

When the dynamics of the environmental scalar field are much slower (e.g., biomass of harmful algae blooms) than those of mobile agents, we may consider that the scalar field is static for the purpose of finding peaks. Suppose that the scalar environmental field $\mu(\nu)$ is generated by a network of radial basis function [9]:

$$\mu(\nu) = \sum_{j=1}^{m} \phi_j(\nu)\theta^j = \phi^T(\nu)\theta, \tag{6}$$

where $\phi^T(\nu)$ and θ are defined respectively by

$$\begin{aligned} \phi^T(\nu) &= \begin{bmatrix} \phi_1(\nu) & \phi_2(\nu) & \cdots & \phi_m(\nu) \end{bmatrix} \in \mathbb{R}^{1\times m}, \\ \theta &= \begin{bmatrix} \theta^1 & \theta^2 & \cdots & \theta^m \end{bmatrix}^T \in \mathbb{R}^{m\times 1}. \end{aligned} \tag{7}$$

Gaussian radial basis functions $\phi_j(\nu)$ are given by

$$\phi_j(\nu) = \frac{1}{\beta_j} \exp\left(\frac{-\|\nu - \xi_j\|^2}{\sigma_j^2} \right), \forall j \in M, \tag{8}$$

where $M := \{1, \cdots, m\}$, σ_j is the width of the Gaussian basis and β_j is a normalizing constant. Centers of basis functions $\{\xi_j | j \in M\}$ are assumed to be uniformly distributed in the surveillance region Q.

One may use the gradient ascent control based on the estimated gradient of $\mu(q)$ to find peaks. To this end, we introduce some notations. The partial derivative of $\phi(x) \in \mathbb{R}^{m\times 1}$ with respect to $x \in \mathbb{R}^{2\times 1}$ evaluated at x^* is denoted by $\phi'(x^*)$ and is given as follows.

$$\phi'(x^*) := \frac{\partial \phi(x)}{\partial x}\Big|_{x=x^*} \in \mathbb{R}^{m\times 2}.$$

The gradient of the field at q_i is denoted by

$$\nabla\mu(q_i) = \frac{\partial \mu(x)}{\partial x}\Big|_{x=q_i} \in \mathbb{R}^{2\times 1}. \tag{9}$$

Using (6), (9) can be represented in terms of θ,

$$\nabla \mu(q_i) = \frac{\partial \phi^T(x)}{\partial x}\Big|_{x=q_i} \theta = \phi'^T(q_i)\theta \in \mathbb{R}^{2\times 1}. \tag{10}$$

The estimate of $\nabla \mu(q_i)$ based on $\hat{\theta}$ is denoted by $\nabla \hat{\mu}(q_i)$.

4 The problem statement

We first review the motivations for our work. The first motivation is to estimate the scalar field of interest and locate the peaks of the field for environmental monitoring. The mobile agent can be equipped with a sensor to measure the scalar value of the field, e.g., Chlorophyll a for gauging the total biomass of algae. In a straightforward application, after finding peaks, the mobile robots can perform a set of necessary tasks to neutralize and/or remove them. The second motivation is to design scalable and distributed coordination algorithms for resource-constrained mobile sensor networks. Recently, developing scalable and distributed estimation and coordination algorithms for multi-agent systems using only local information from local neighboring agents has been one of the most fundamental problems in coordinating mobile robotic sensors [1, 3, 4, 9]. This is an important research direction such that the complexity of the algorithm will not increase as the number of robotic sensors increases. Therefore, although each agent has limited capabilities, as a group, they can perform various tasks at a level which is compatible to a small number of high-end mobile agent. Finally, the conditions for which the convergence is guaranteed need to be prescribed for users.

From the aforementioned motivations, the problem of this paper is stated as follows. For the multi-agent system described in Section 2 and the scalar field model presented in Section 3, the problem is to synthesize scalable and distributed coordination algorithms such that the multi-agent system estimates the field and locates peaks of the field in a collective manner. Moreover, convergence properties of the proposed coordination algorithms need to be analyzed and the conditions for which the convergence is guaranteed need to be identified.

5 Coordination algorithms

In this section, we provide a solution to the problem formulated in Section 4. For agents to make distributed sampling and to maintain the connectivity, a flocking algorithm as described in Section 5.1 will be applied. The overall distributed adaptive control is proposed in Section 5.2 based on recursive scalar field estimators. The collective closed-loop multi-agent system is formulated in Section 5.3. Finally convergence properties of the multi-agent system under the proposed strategies are analyzed in Section 5.4.

5.1 A distributed flocking algorithm

In order for multiple agents to sample a scalar field at spatially distributed locations simultaneously, a group of mobile agents will be coordinated by a flocking algorithm [6, 2, 5, 9]. In addition, swarming or flocking behavior helps to maintain the communication graph connected among the group of agents. The algorithm consists of the three flocking rules: Cohesion: try to stay close to neighbors; Separation: avoid collisions with neighbors; Alignment: try to match velocity with neighbors.

We use attractive and repulsive potential functions similar to ones used in [5, 2, 9] to achieve flocking rules of cohesion and separation. Toward this end, we use a collective potential function [9]

$$\begin{aligned} U_1(q) &:= \sum_i \sum_{j \in \mathcal{N}(i,q), j \neq i} U_{ij}(\|q_i - q_j\|^2) \\ &= \sum_i \sum_{j \in \mathcal{N}(i,q), j \neq i} U_{ij}(r_{ij}), \end{aligned} \tag{11}$$

where $r_{ij} := \|q_i - q_j\|^2$. The pair-wise attractive/repulsive potential function $U_{ij}(\cdot)$ in (11) is defined by

$$U_{ij}(r_{ij}) := \frac{1}{2}\left(\ln(\alpha + r_{ij}) + \frac{\alpha + d^2}{\alpha + r_{ij}}\right), \text{ if } r_{ij} < d_0^2,$$

otherwise (i.e., $r_{ij} \geq d_0^2$), it is defined according to the gradient of the potential, which will be described shortly. Here $\ln(x)$ denotes the natural logarithm of x to the base e. $\alpha, d \in \mathbb{R}_{>0}$ and

$d < d_0$. The gradient of the potential with respect to q_i for agent i is given by

$$\nabla U_1(q_i) := \frac{\partial U_1(q)}{\partial \tilde{q}_i}\Big|_{\tilde{q}_i = q_i} = \sum_{j \neq i} \frac{\partial U_{ij}(r)}{\partial r}\Big|_{r=r_{ij}} (q_i - q_j)$$

$$= \begin{cases} \sum_{j \neq i} \frac{(r_{ij} - d^2)(q_i - q_j)}{(\alpha + r_{ij})^2} & \text{if } r_{ij} < d_0^2 \\ \sum_{j \neq i} \rho\left(\frac{\sqrt{r_{ij}} - d_0}{|d_1 - d_0|}\right) \frac{\|d_0^2 - d^2\|}{(\alpha + d_0^2)^2}(q_i - q_j) & \text{if } r_{ij} \geq d_0^2, \end{cases}$$

where $\rho : \mathbb{R}_{\geq 0} \rightarrow [0, 1]$ is the bump function [2]

$$\rho(z) := \begin{cases} 1, & z \in [0, h); \\ \frac{1}{2}\left[1 + \cos\left(\pi \frac{(z-h)}{(1-h)}\right)\right], & z \in [h, 1]; \\ 0, & \text{otherwise.} \end{cases}$$

A potential U_2 [9] is also used to model the environment. U_2 enforces each agent to stay inside the closed and connected surveillance region in Q and prevents collisions with obstacles in Q. We construct U_2 such that it is radially unbounded in q, i.e., $U_2(q) \rightarrow \infty$ as $\|q\| \rightarrow \infty$. This condition will be used for making a Lyapunov function candidate radially unbounded. Define the total artificial potential by

$$U(q) := k_1 U_1(q) + k_2 U_2(q), \tag{12}$$

where $k_1, k_2 \in \mathbb{R}_{>0}$ are weighting factors.

The flocking rule of alignment will be implemented by adding velocity consensus that minimizes a quadratic disagreement function. The quadratic disagreement function $\Psi_G : \mathbb{R}^{2n} \rightarrow \mathbb{R}_{\geq 0}$ is used to evaluate the group disagreement in the network of agents

$$\Psi_G(p) := \frac{1}{4} \sum_{(i,j) \in \mathcal{E}(q)} a_{ij} \|p_j - p_i\|^2,$$

where $p := \mathrm{col}(p_1, p_2, \cdots, p_n) \in \mathbb{R}^{2n}$. The disagreement function [2, 18] can be expressed via the Laplacian $\hat{L}_2$: $\Psi_G(p) = \frac{1}{2} p^T \hat{L}_2 p$, and hence the gradient of $\Psi_G(p)$ w.r.t. p is given by $\nabla \Psi_G(p) = \hat{L}_2 p$.

5.2 Distributed adaptive control

In this subsection, we propose a distributed adaptive control algorithm. The adaptive control law for each agent will be generated using only local information from neighboring agents. Recall that the dynamics of agent i in (5) is given by

$$\dot{q}_i(t) = p_i(t),$$
$$\dot{p}_i(t) = u_i(t),$$

where $u_i(t)$ is the input of agent i. The control input $u_i(t)$ is then proposed as follows.

$$\begin{aligned} u_i(t) = & -\nabla U(q_i(t)) - \nabla\Psi_G(p_i(t)) - k_{d_i} p_i(t) \\ & + k_4 \phi'^T(q_i(t))\hat{\theta}_i(t), \end{aligned} \tag{13}$$

where the first two terms of the right-hand side of (13) provide the swarming effort as discussed in Section 5.1. The third term in (13) provides damping. $\hat{\theta}_i(t)$ is the estimate of $\theta(t)$ by agent i using a recursive parameter estimation algorithm. In what follows, two of such adaptation laws are proposed.

To achieve a consensus between estimates, the gradient of the disagreement function at $\hat{\theta}_i(t)$ will be used in the adaptation laws, which is given by

$$\nabla\Psi_G(\hat{\theta}_i(t)) = \sum_{j\in\mathcal{N}_i} a_{ij}(q(t))(\hat{\theta}_i(t) - \hat{\theta}_j(t)),$$

here the quadratic disagreement function $\Psi_G(\hat{\theta}_d(t))$: $\mathbb{R}^{mn} \to \mathbb{R}_{\geq 0}$ is defined as

$$\Psi_G(\hat{\theta}_d(t)) = \frac{1}{4}\sum_{(i,j)\in\mathcal{E}(q)} a_{ij} \parallel \hat{\theta}_j(t) - \hat{\theta}_i(t) \parallel^2 = \frac{1}{2}\hat{\theta}_d^T(t)\hat{L}_m\hat{\theta}_d(t),$$

where $\hat{L}_m = L \otimes I_m$, and $\hat{\theta}_d(t) = \text{col}(\hat{\theta}_1(t), \cdots, \hat{\theta}_n(t))$.

To develop estimators, the error vector $e_i(t)$ of agent i between the estimated values and measured values is defined by

$$e_i(t) = -\begin{bmatrix} \hat{\mu}_i(q_i(t)) - \mu(q_i(t)) \\ \hat{\mu}_i(q_j(t)) - \mu(q_j(t)) \\ \vdots \\ \hat{\mu}_i(q_k(t)) - \mu(q_k(t)) \end{bmatrix},$$

and can be rewritten by

$$e_i(t) = -\begin{bmatrix} \phi^T(q_i(t))\tilde{\theta}_i(t) \\ \phi^T(q_j(t))\tilde{\theta}_i(t) \\ \vdots \\ \phi^T(q_k(t))\tilde{\theta}_i(t) \end{bmatrix} = -\Phi_i(t)\tilde{\theta}_i(t),$$

where

$$\Phi_i(t) = \begin{bmatrix} \phi^T(q_i(t)) \\ \phi^T(q_j(t)) \\ \vdots \\ \phi^T(q_k(t)) \end{bmatrix} \in \mathbb{R}^{|\overline{\mathcal{N}}_i| \times m},$$

with $j, \cdots, k \in \mathcal{N}_i$.

With the aforementioned notations, we propose that agent i updates $\hat{\theta}_i(t)$ based on the following two adaptation laws.

- Using the gradient-based estimator, $\hat{\theta}_i(t)$ is updated by the following adaptation law.

$$\dot{\hat{\theta}}_i(t) = \gamma_i \Phi_i^T(t) e_i(t) - \gamma_i k_4 \phi'(q_i(t)) p_i(t) - k_6 \gamma_i \nabla \Psi_G(\hat{\theta}_i(t)), \tag{14}$$

  where γ_i is the estimation gain and k_6 is a consensus gain for parameter estimates.

- Using the recursive least squares (RLS) estimator, $\hat{\theta}_i(t)$ is updated by the following adaptation law.

$$\begin{aligned} \dot{\hat{\theta}}_i(t) =& P_i \Phi_i^T(t) e_i(t) - P_i k_4 \phi'(q_i(t)) p_i(t) \\ &- k_6 P_i \nabla \Psi_G(\hat{\theta}_i(t)), \\ \dot{P}_i(t) =& - P_i(t) \Phi_i^T(t) \Phi_i(t) P_i(t), \end{aligned} \tag{15}$$

  where $P_i(t)$ is defined by

$$P_i(t) = \left(\int_0^t \Phi_i^T(\tau) \Phi_i(\tau) d\tau \right)^{-1} \in \mathbb{R}^{m \times m}.$$

5.3 Collective dynamics of all agents

In this subsection, we derive the collective dynamics of all agents under the proposed coordination algorithms using a collective cost function. The collective cost function $C_d(q(t))$ for all agents is defined by

$$\begin{aligned} C_d(q(t)) &= k_4 \sum_{i \in \mathcal{I}} [\mu_{max} - \mu(q_i(t))] \\ &= k_4 \sum_{i \in \mathcal{I}} [\mu_{max} - \phi^T(q_i(t))\theta]. \end{aligned}$$

The collective estimate of $C_d(q(t))$ by all agents at time t is $\hat{C}_d(q(t))$ and is given by

$$\begin{aligned} \hat{C}_d(q(t)) &= k_4 \sum_{i \in \mathcal{I}} [\mu_{max} - \hat{\mu}_i(q_i(t))] \\ &= k_4 \sum_{i \in \mathcal{I}} [\mu_{max} - \phi^T(q_i(t))\hat{\theta}_i(t)], \end{aligned}$$

where the estimate of $\mu(\nu)$ at ν in (6) by agent i is denoted by $\hat{\mu}_i(\nu)$ and is given as $\hat{\mu}_i(\nu) := \phi^T(\nu)\hat{\theta}_i(t)$. The gradient of C_d at $q(t)$ is given by

$$\nabla C_d(q(t)) = -k_4 \begin{bmatrix} \phi'^T(q_1(t)) \\ \phi'^T(q_2(t)) \\ \vdots \\ \phi'^T(q_n(t)) \end{bmatrix} \theta = -A_d(t)\theta_d,$$

where $\theta_d := \mathbf{1}_n \otimes \theta$. $A_d(t)$ is defined by

$$A_d(t) = k_4 \text{diag}(\phi'^T(q_1(t)), \cdots, \phi'^T(q_n(t))) \in \mathbb{R}^{2n \times mn}.$$

The collective estimate of $\nabla C_d(q(t))$ by all agents is denoted by $\nabla \hat{C}_d(q(t))$ and is given by

$$\nabla \hat{C}_d(q(t)) = -k_4 \begin{bmatrix} \phi'^T(q_1(t))\hat{\theta}_1(t) \\ \vdots \\ \phi'^T(q_n(t))\hat{\theta}_n(t) \end{bmatrix} = -A_d(t)\hat{\theta}_d(t).$$

The collective dynamics of all agents from (5) and (13) are given by

$$\begin{aligned} \dot{q}(t) &= p(t), \\ \dot{p}(t) &= -\nabla U(q(t)) - \nabla \Psi_G(p(t)) - K_d p(t) - \nabla \hat{C}_d(q(t)), \end{aligned} \tag{16}$$

where $q(t) = \text{col}(q_1(t), \cdots, q_n(t))$, and $p(t) = \text{col}(p_1(t), \cdots, p_n(t))$.

The collective version of the adaptive law in (14) for all agents is given by

$$\dot{\hat{\theta}}_d(t) = \Gamma_d \Phi_d^T(t) e_d(t) - \Gamma_d A_d^T(t) p(t) - \Gamma_d \hat{L}_m \hat{\theta}_d(t), \tag{17}$$

where $\Gamma_d = \Gamma \otimes I_m$ and $\Gamma = \Gamma^T \succ 0$ is the diagonal matrix given by $\Gamma = \text{diag}(\gamma_1, \cdots, \gamma_n)$. Notice that $\hat{L}_m \hat{\theta}_d(t) = \hat{L}_m \tilde{\theta}_d(t)$ in (17). The collective error $e_d(t)$ is defined as

$$e_d(t) = \begin{bmatrix} e_1(t) \\ \vdots \\ e_n(t) \end{bmatrix} = \begin{bmatrix} -\Phi_1(t)\tilde{\theta}_1(t) \\ \vdots \\ -\Phi_n(t)\tilde{\theta}_n(t) \end{bmatrix} = -\Phi_d(t)\tilde{\theta}_d(t), \tag{18}$$

where $\Phi_d(t) = \text{diag}(\Phi_1(t), \cdots, \Phi_n(t)) \in \mathbb{R}^{\left(\sum_{i \in \mathcal{I}} |\overline{\mathcal{N}}_i|\right) \times mn}$.

The collective version of the adaptive law in (15) for all agents is given by

$$\begin{aligned} \dot{\hat{\theta}}_d(t) =& - P_d(t)\Phi_d^T(t)\Phi_d(t)\tilde{\theta}_d(t) \\ & - P_d(t) A_d^T(t) p(t) - P_d(t)\hat{L}_m \hat{\theta}_d(t), \\ \dot{P}_d(t) =& - P_d(t)\Phi_d^T(t)\Phi_d(t) P_d(t). \end{aligned} \tag{19}$$

where $P_d(t)$ is defined by $P_d(t) = \text{diag}(P_1(t), \cdots, P_n(t)) \in \mathbb{R}^{mn \times mn}$.

5.4 Convergence analysis

In this section, we present the results for convergence properties of the proposed multi-agent systems. To this end, we define the global performance cost function of the multi-agent system with the gradient-based algorithm in (17)

$$V_d(q(t), p(t), \tilde{\theta}_d(t)) = U(q(t)) + \frac{p^T(t)p(t)}{2} + C_d(q(t)) + \frac{\tilde{\theta}_d^T(t)\Gamma_d^{-1}\tilde{\theta}_d(t)}{2}, \tag{20}$$

where $\tilde{\theta}_d(t) = \text{col}(\tilde{\theta}_1(t), \cdots, \tilde{\theta}_n(t))$ is the estimation error vector defined by $\tilde{\theta}_d(t) := \hat{\theta}_d(t) - \theta_d$. The global performance cost function for the RLS algorithm in (19) is defined by

$$V_d(q(t), p(t), \tilde{\theta}_d(t)) = U(q(t)) + \frac{p^T(t)p(t)}{2} + C_d(q(t)) + \frac{\tilde{\theta}_d^T(t) P_d^{-1}(t)\tilde{\theta}_d(t)}{2}. \tag{21}$$

The collective performance cost function will be minimized by agents. The convergence properties of the multi-agent system is summarized by the following theorem.

Theorem 1 *We consider the distributed control law in* (13) *based on the gradient-based estimator in* (14) *(respectively, the RLS estimator in* (15)*) along with the global performance cost function* V_d *in* (20) *(respectively,* (21)*). For any initial state* $x_0 = col(q_0, p_0, \tilde{\theta}_{d_0}) \in D_d$*, where* D_d *is a compact set. Let* $D_{Ad} = \{x \in D \mid V_d(x) \leq a\}$ *be a level-set of the collective cost function. Let* D_{cd} *be the set of all points in* D_{Ad}*, where* $\frac{dV_d(x)}{dt} = 0$*. Then every solution starting from* D_{Ad} *approaches the largest invariant set* M_d *contained in* D_{cd} *as* $t \to \infty$*.*

Moreover, for the adaptive control using the gradient-based estimator (respectively, the RLS estimator), if $(\hat{L}_2 + K_d)$ *and* $(\Phi_d^T(t)\Phi_d(t) + \hat{L}_m)$ *(respectively,* $(\frac{1}{2}\Phi_d^T(t)\Phi_d(t) + \hat{L}_m)$*) are positive definite, then any point* $x^* = col(q^*, 0, 0)$ *in* M_d *is a critical point of the cost function* $V_d(x)$*, which implies that* x^* *is either a (local) minimum of* $V_d(x)$ *or an inflection point,*

$$\left.\frac{\partial V_d(x)}{\partial x}\right|_{x=x^*} = 0,$$

and $\hat{\theta}_d(t)$ *converges to* θ_d *as* $t \to \infty$*.*

Proof of Theorem 1 in the case of the gradient-based estimator.

Using (16), the time derivative of $V_d(x)$ in (20) is obtained by

$$\begin{aligned}\dot{V}_d = &\begin{bmatrix} \nabla U(q(t)) + \nabla C_d(q(t)) \\ p(t) \end{bmatrix}^T \begin{bmatrix} p(t) \\ -\nabla U(q(t)) - \nabla \Psi_G(p(t)) - K_d p(t) - \nabla \hat{C}_d(q(t)) \end{bmatrix} \\ &+ \tilde{\theta}_d^T(t)\Gamma_d^{-1}\dot{\hat{\theta}}_d(t) \\ = &- p^T(t)(\hat{L}_2 + K_d)p(t) + \tilde{\theta}_d^T(t)(A_d^T(t)p(t) + \Gamma_d^{-1}\dot{\hat{\theta}}_d(t)).\end{aligned} \tag{22}$$

With (17) and (22), we obtain

$$\dot{V}_d = -p^T(t)(\hat{L}_2 + K_d)p(t) - \tilde{\theta}_d^T(t)(\Phi_d^T(t)\Phi_d(t) + \hat{L}_m)\tilde{\theta}_d(t) \leq 0. \tag{23}$$

Let $x(t) = \mathrm{col}(q(t), p(t), \tilde{\theta}_d(t))$. From (20), we conclude that $V_d(x(t))$ is radially-unbounded, i.e., $V_d(x(t)) \to \infty$ as $\|x(t)\| \to \infty$. Hence, $D_{Ad} = \{x(t) \mid V_d(x(t)) \leq a\}$ is bounded and D_{Ad} with $\frac{d}{dt}V_d(x) \leq 0$ in (23) for all $x \in D_{Ad}$ is a positively invariant set. By LaSalle's invariant principle every point $x(t)$ in D_{Ad} approaches M_d included in D_{cd} which is given by

$$M_d := \{x(t) \mid \dot{V}_d = -p^T(t)(\hat{L}_2 + K_d)p(t) - \tilde{\theta}_d^T(t)(\Phi_d^T(t)\Phi_d(t) + \hat{L}_m)\tilde{\theta}_d(t) = 0\}, \tag{24}$$

as $t \to \infty$. Let x^* be a solution that belongs to D_{cd}. If $(\hat{L}_2 + K_d) \succ 0$ and $(\Phi_d^T(t)\Phi_d(t) + \hat{L}_m) \succ 0$, $\forall x \in D_d$, from (24), any point x^* in M_d is the form of $x^*(t) = \text{col}(q^*(t), p^* \equiv 0, \tilde{\theta}_d^* \equiv 0)$.

$$\tilde{\theta}_d^* \equiv 0 \Rightarrow 0 \equiv \hat{\theta}_d^*(t) - \theta_d \Rightarrow \nabla \hat{C}_d(q^*) \equiv \nabla C_d(q^*).$$

From (16), we have

$$\tilde{\theta}_d^* \equiv 0,\, p^*(t) \equiv 0 \Rightarrow \dot{q}^*(t) \equiv 0 \Rightarrow 0 \equiv -\nabla U(q^*) - \nabla \hat{C}_d(q^*).$$

This implies that x^* is a critical point of the cost function $V_d(x)$ and $\hat{\theta}_d(t)$ converges to θ_d. QED.

Proof of Theorem 1 in the case of the RLS estimator.

Using (16), the time derivative of $V_d(x)$ in (21) is obtained by

$$\begin{aligned}
\dot{V}_d = & \begin{bmatrix} \nabla U(q(t)) + \nabla C_d(q(t)) \\ p(t) \end{bmatrix}^T \begin{bmatrix} p(t) \\ -\nabla U(q(t)) - \nabla \Psi_G(p(t)) - K_d p(t) - \nabla \hat{C}_d(q(t)) \end{bmatrix} \\
& + \tilde{\theta}_d^T(t) P_d^{-1}(t) \dot{\hat{\theta}}_d(t) + \frac{\tilde{\theta}_d^T(t) \dot{P}_d^{-1} \tilde{\theta}_d}{2}(t) \\
= & - p^T(t)(\hat{L}_2 + K_d)p(t) \\
& + \tilde{\theta}_d^T(t)(A_d^T(t)p(t) + P_d^{-1}(t)\dot{\hat{\theta}}_d(t)) \\
& + \frac{1}{2}\tilde{\theta}_d^T(t)\frac{dP_d^{-1}(t)}{dt}\tilde{\theta}_d(t).
\end{aligned} \tag{25}$$

With (19) and (25), we obtain

$$\dot{V}_d = -p^T(t)(\hat{L}_2 + K_d)p(t) - \tilde{\theta}_d^T(t)\left(\frac{1}{2}\Phi_d^T(t)\Phi_d(t) + \hat{L}_m\right)\tilde{\theta}_d(t) \le 0. \tag{26}$$

The rest of the proof follows as in the case of the gradient estimator. QED.

6 A sampling scheme for helping convergence

To improve the possibility of satisfying the sufficient conditions of convergence in Theorem 1, we provide a sampling scheme that will help on making $\Phi_d^T(t)\Phi_d(t)$ positive definite.

Table 1: Parameters in the simulation

Parameters	Values
Number of agents n	30
Number of basis functions m	9
Surveillance region Q	$[0,3]^2$
(d, d_0, d_1, r)	$(0.3, 0.39, 0.5, 0.5)$
(k_1, k_2, k_4, k_6)	$(5, 1, 1, 1)$
k_d	$5I_{2n}$
$P(0) = \Gamma$	$0.5I_m$
$\hat{\theta}_i(0)$	$0_{m\times 1}$
α	0.05

In this sampling scheme, at every sampling time t, a fixed number (m) of measurements sampled previously will be augmented to the fresh measurements available at time t for agent i. The selection of such m additional measurements at time t for agent i is as follows.

$$\bar{q}_{ij}(t) = \arg\min_{q\in\Omega_i(t)} \|q - \xi_j\|, \quad \forall j \in M, \tag{27}$$

where $M := \{1, \cdots, m\}$ and ξ_j is the center location of the j-th kernel as defined in (8). $\Omega_i(t)$ is defined by

$$\Omega_i(t) := \left(\bigcup_{k\in\bar{\mathcal{N}}_i(t)} \{\bar{q}_{ij}(t^-) \mid j \in M\} \right) \cup \left(\bigcup_{k\in\bar{\mathcal{N}}_i(t^-)} q_k(t^-) \right),$$

where t^- is the sampling time taken prior to t. Notice that this selection process in (27) is scalable and distributed.

Expanded $\Phi_i(t)$ due to the the augmented sampled data at time t is as follows.

$$\Phi_i(t) = \begin{bmatrix} \phi(q_i(t)) & \cdots & \phi(\bar{q}_{i1}(t)) & \cdots & \phi(\bar{q}_{im}(t)) \end{bmatrix}^T \in \mathbb{R}^{|\overline{\mathcal{N}}_i+m|\times m}.$$

7 Simulation results

We have applied the proposed distributed adaptive control to fully actuated nonholonomic differentially driven mobile robots introduced in Section 2.1 under different conditions. For the numerical simulation study, two scalar fields illustrated as color maps in Fig. 3 were generated by the model in (6) with nine radial basis functions, i.e., $m = 9$. Agents were launched at a set of randomly distributed initial poses (positions and angles). Two sets of scalar fields and initial poses (2×2 combinatorial scenarios) were selected and used for all simulations for a fair comparison. Initial poses of agents and scalar fields have been named 1 and 2 for more clarification. A limited transmission radius was chosen to be $r = 0.5$. The initial value for the parameter vector of each agent was given as a zero vector, i.e., $\hat{\theta}_i(0) = 0_{m\times 1} \in \mathbb{R}^m$. Table 1 shows the parameters commonly used for the numerical evaluation.

7.1 Gradient and RLS estimators

Figs. 3(a), (b), (c), and (d) show trajectories of agents with the distributed adaptive control using the gradient-based estimator under initial conditions 1 and 2 and fields 1 and 2 (2×2 scenarios). The trajectories of robots are marked by snapshots of poses at $t = 0$ sec., $t = 100$ sec., and $t = 1000$ sec., by white, magenta, and black arrowheads, respectively, showing their positions and heading angles. The additional sampling positions are marked by stars ($*$). Each agent runs its own control based on its own estimation of θ fusing its and neighbors' measurements in a distributed manner.

To evaluate the convergence rate of the parameter estimation for each agent, we compute the error norm $\|\tilde{\theta}_i(t)\|$, where $\tilde{\theta}_i(t) := \hat{\theta}_i(t) - \theta$ for agent i, and plot $\|\tilde{\theta}_i(t)\|$ for all agents $i \in \mathcal{I}$ with respect to time t as in Figs. 4(a), (b), (c), and (d) for adaptive control with the gradient-based under 2×2 combinatorial scenarios.

Under the limited communication range, different groups of agents are formed to share measurements and interact each other in a distributed fashion. Therefore, the final configuration and convergence rate of each agent will depend on the initial positions of the multi-agent system and the uncertain scalar field as shown in Figs. 3 and 4. In particular, comparing Fig. 3(a) and Fig. 3(c), it is observed that initial poses of agents play an important role on the final configuration of agents. For example, the initial positions of agents are separated in two groups in Fig. 3(c), therefore these two groups cannot communicate, resulting that one group of agents converge to a closest local maximum. This can be also seen in Figs. 4(a) and (c) in which parameter estimates by agents Fig. 4(c) did not converge to the correct parameters since the communication graph is not connected due to the limited communication range and the initial poses of agents. The pairs of behaviors under initial poses 1 and 2 as shown in Fig. 3(b) and Fig. 3(d), and Fig. 4(b) and Fig. 4(d) clearly show the similar effect of the initial positions of robots on the final configuration of agents.

Figs. 5(a), (b), (c), and (d) show trajectories of agents using distributed adaptive control based on the RLS estimator under 2×2 combinatorial scenarios. Comparing Figs. 3 and 5, there is not too much difference between trajectories obtained with gradient-based and RLS estimators. Figs. 6(a), (b), (c), and (d) show the parameter convergence rate of each agent using distributed adaptive control based on the RLS estimator under 2×2 combinatorial scenarios.

From simulation results in Figs. 3, 4, 5, and 6, we see that agents with distributed adaptive control and learning algorithms successfully found major peaks of the uncertain fields. Note again that some of agents would converge to the local minima of the field.

7.2 Without the proposed sampling scheme

To evaluate the effectiveness of the sampling scheme proposed in (27), we compare distributed adaptive control based on the gradient-based estimator with and without the sampling scheme.

Trajectories of agents with the distributed adaptive control based on the gradient-based estimator with using sampling scheme proposed in (27) are shown in Figs. 3(a), (b), (c), and (d) and ones without using sampling scheme are shown in Figs. 7(a), (b), (c), and (d) over 2×2 combinatorial scenarios. The multi-agent system with the proposed sampling scheme outperforms the multi-agent system without the sampling scheme as can be seen clearly by comparing parameter error convergence rates in Figs. 4 and 8.

7.3 Randomized initial values for $\hat{\theta}_i(0)$

Each agent starts by an initial guess of $\hat{\theta}_i(0)$ and recursively updates it by new measurements collected from itself and its neighbors. Using zero initial conditions may be plausible in detecting accidental release of toxic chemical plumes, which is not supposed to be found in the surveillance region in a normal situation. On the other hand, using randomized initial conditions can be viewed as exploratory behaviors by dispatching multiple agents in random directions initially to find peaks rather than letting them move when they find gradient of the field, i.e., the case with zero initial conditions.

So far, we have used initial values $\hat{\theta}_i(0) = 0_{m\times 1} \in \mathbb{R}^m$ for all simulations under all scenarios illustrated in Figs. 3, 4, 5, and 7.

In order to show the effect of randomized initial values for $\hat{\theta}_i(0)$, we have performed such simulations with randomized initial values for $\hat{\theta}_i(0)$ and their simulation results are shown in Figs. 9 and 10.

In this case, we have observed that the multi-agent system successfully found major peaks, showing similar behaviors and convergence results with respect to the previous results shown in Figs. 3 and 4. We also observed that the simulation results under the randomized initial parameter values yield more consistent final configurations with respect to different initial poses.

8 Conclusions

In this paper, we designed and analyzed a class of multi-agent systems that locate peaks of static scalar fields of interest based on adaptive control. Each agent was driven by swarming and gradient ascent efforts based on its own recursively estimated field via locally collected measurements. The convergence properties of the proposed multi-agent systems were analyzed. A sampling scheme to help the convergence was provided. The simulation results under different scenarios matched well with the predicted behaviors from the convergence analysis, and demonstrated the usefulness of the proposed coordination and sampling algorithms. The proposed multi-agent systems and coordination algorithms were developed under a set of assumptions such as fully actuated nonholonomic

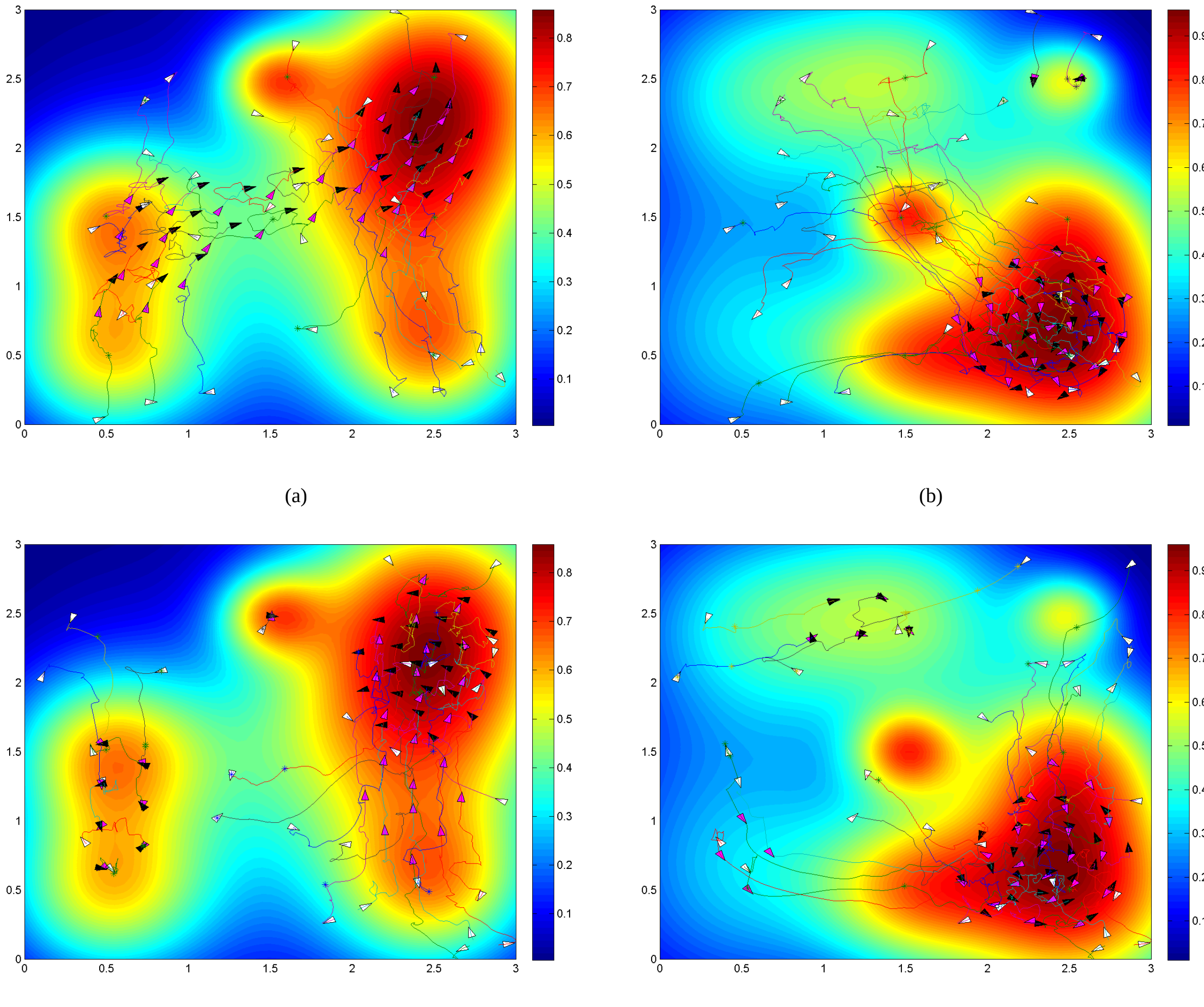

(a) (b) (c) (d)

Figure 3: Trajectories of agents with the distributed adaptive control based on the gradient-based estimator. The trajectories of robots are marked by snapshots of poses at $t = 0$ sec., $t = 100$ sec., and $t = 1000$ sec., by white, magenta, and black arrowheads, respectively, showing their positions and heading angles. The additional sampling positions are marked by stars ($*$). (a) initial pose 1 and field 1, (b) initial pose 1 and field 2, (c) initial pose 2 and field 1, (d) initial pose 2 and field 2. Horizontal and vertical and axes are x and y coordinates respectively and the background color plot shows the scalar field.

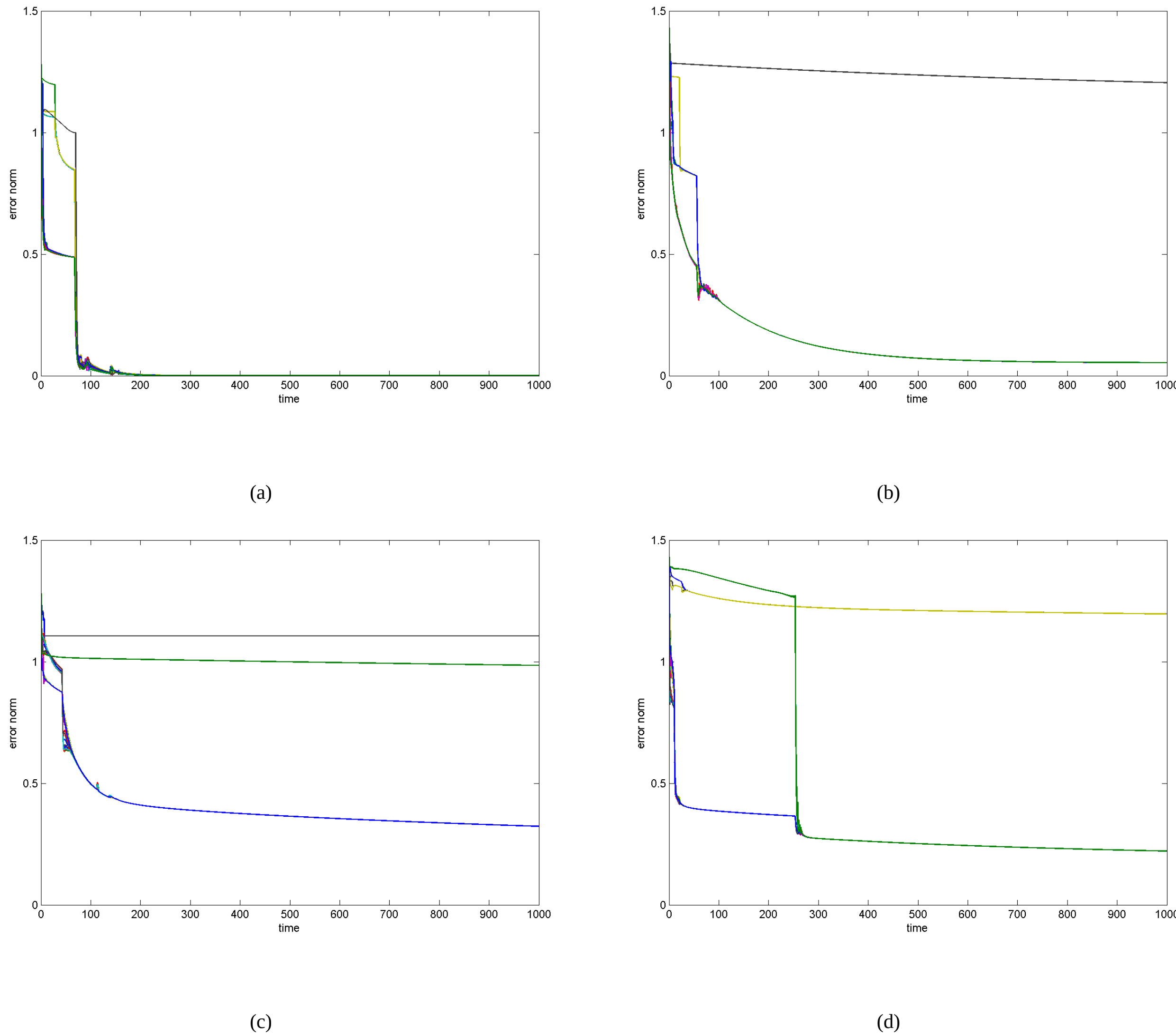

Figure 4: The norm of parameter estimation error, i.e., $\{\|\tilde{\theta}_i(t)\|\}$ by each agent with the distributed adaptive control based on the gradient-based estimator v.s. time. (a) initial pose 1 and field 1, (b) initial pose 1 and field 2, (c) initial pose 2 and field 1, (d) initial pose 2 and field 2.

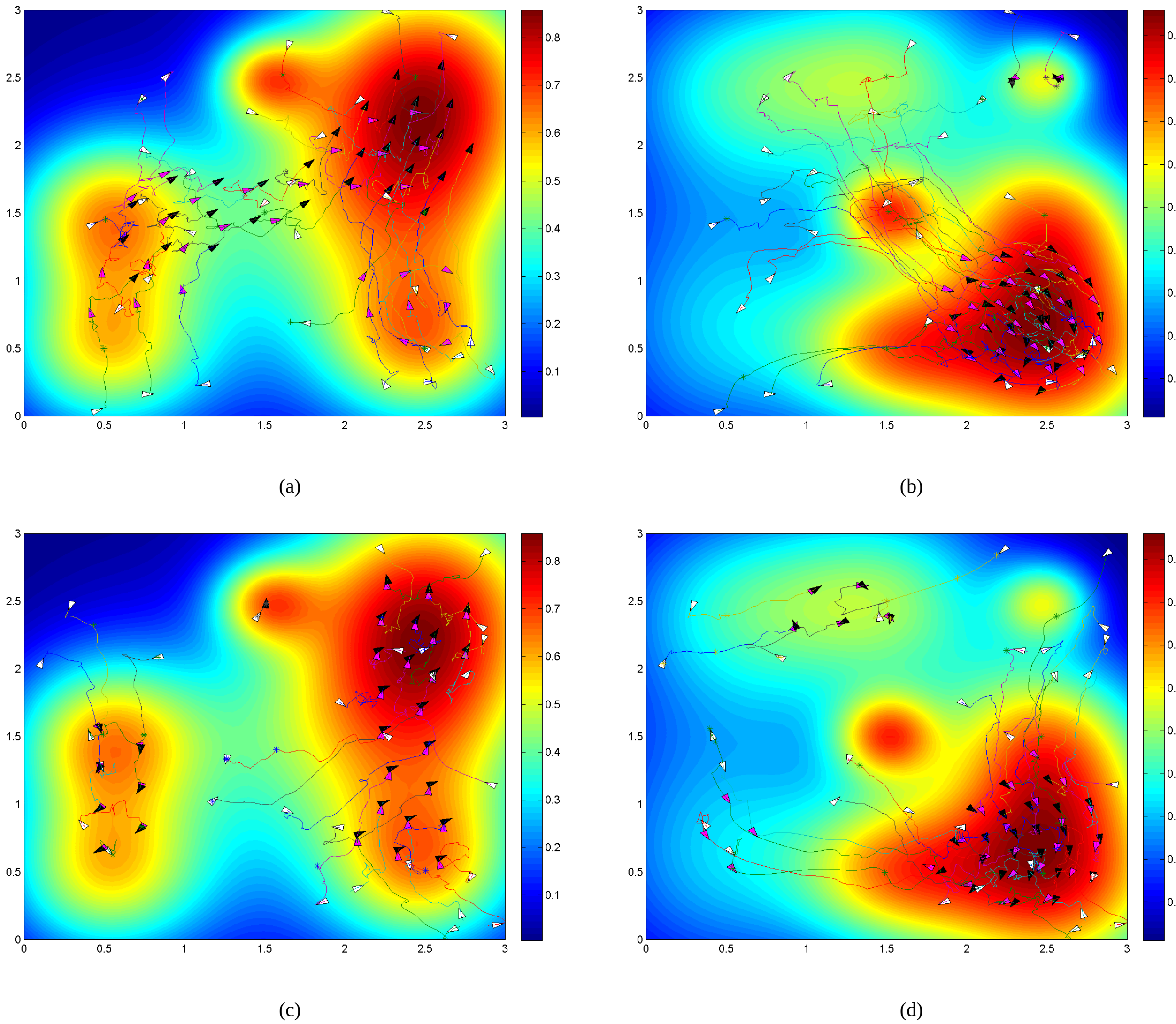

Figure 5: Trajectories of agents with the distributed adaptive control based on the RLS estimator. (a) initial pose 1 and field 1, (b) initial pose 1 and field 2, (c) initial pose 2 and field 1, (d) initial pose 2 and field 2. The same notations are used as in Fig. 3(a).

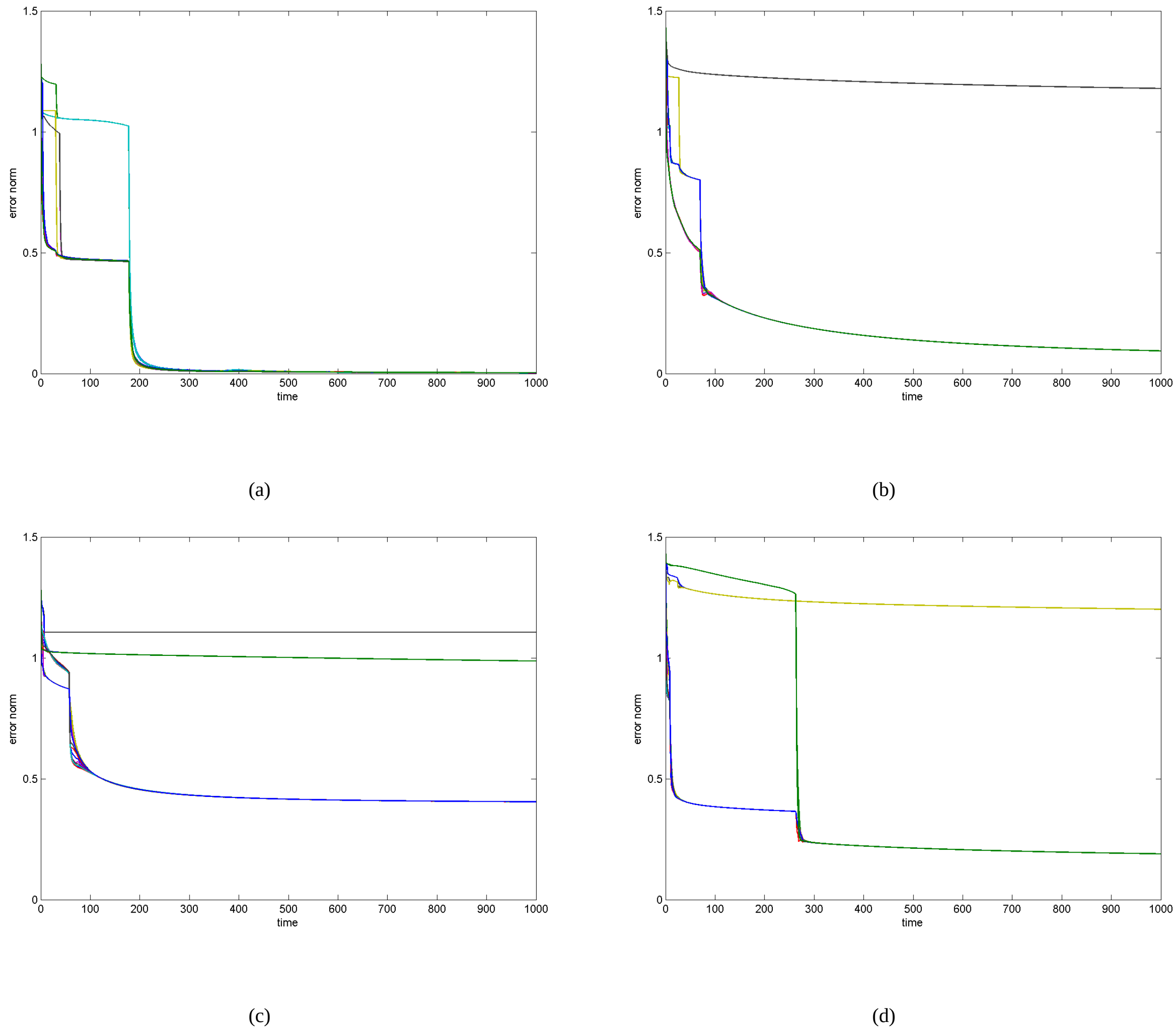

Figure 6: The norm of parameter estimation error, i.e., $\{\|\tilde{\theta}_i(t)\|\}$ by each agent with the distributed adaptive control based on the RLS estimator v.s. time. (a) initial pose 1 and field 1, (b) initial pose 1 and field 2, (c) initial pose 2 and field 1, (d) initial pose 2 and field 2.

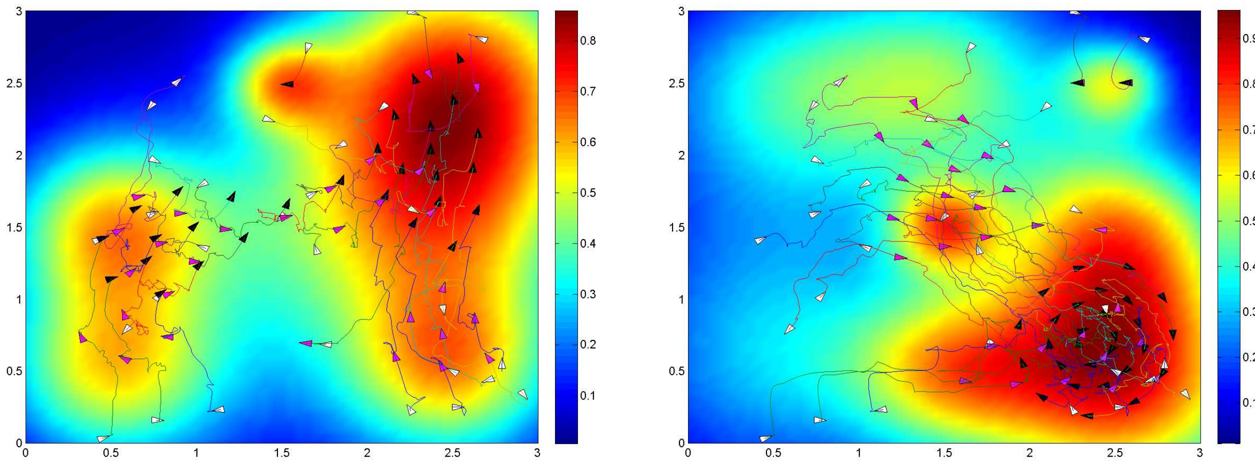

(a) (b)

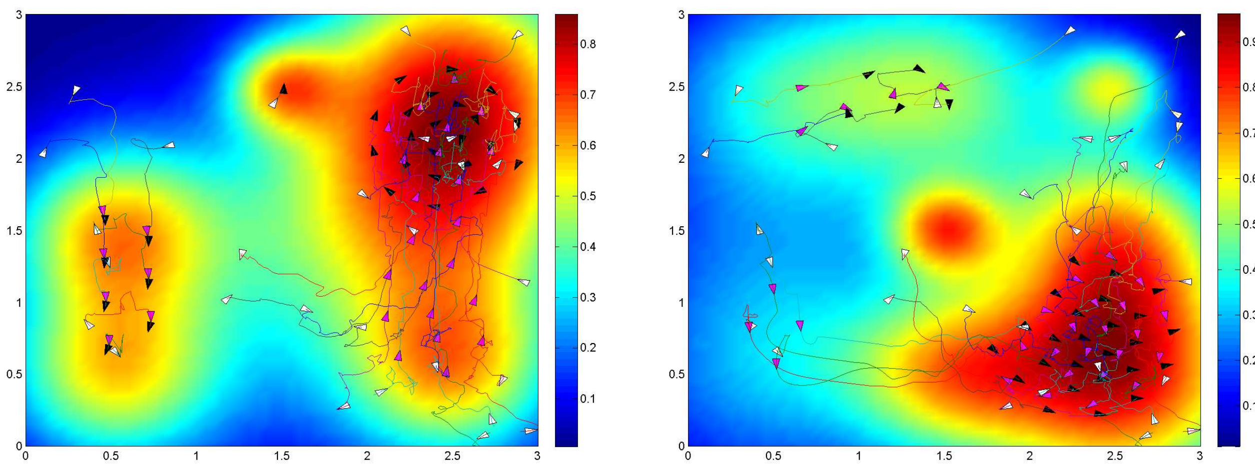

(c) (d)

Figure 7: Trajectories of agents with the distributed adaptive control based on the gradient-based estimator without using sampling scheme proposed in (27). (a) initial pose 1 and field 1, (b) initial pose 1 and field 2, (c) initial pose 2 and field 1, (d) initial pose 2 and field 2. The same notations are used as in Fig. 3(a).

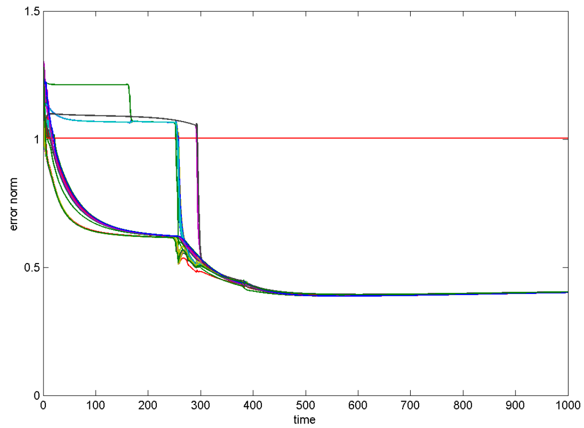

(a)

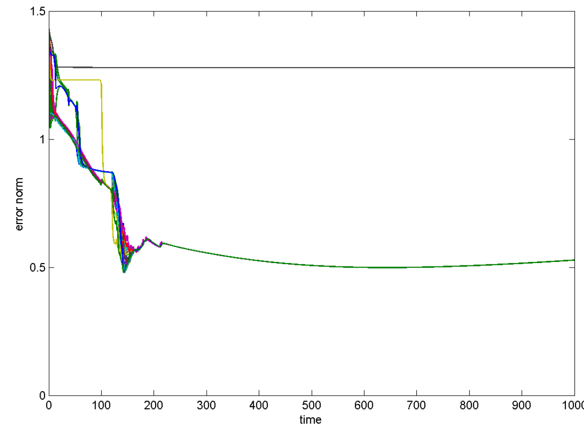

(b)

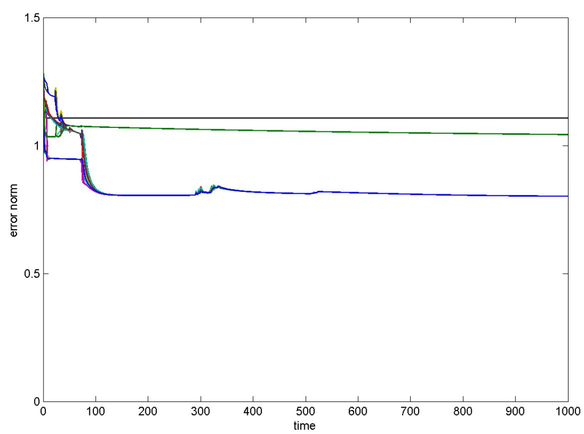

(c)

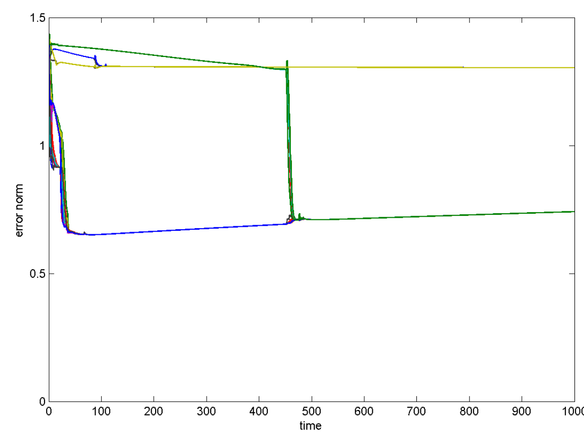

(d)

Figure 8: The norm of parameter estimation error, i.e., $\{\|\tilde{\theta}_i(t)\|\}$ by each agent with the distributed adaptive control based on the gradient-based estimator without using sampling scheme v.s. time. (a) initial pose 1 and field 1, (b) initial pose 1 and field 2, (c) initial pose 2 and field 1, (d) initial pose 2 and field 2.

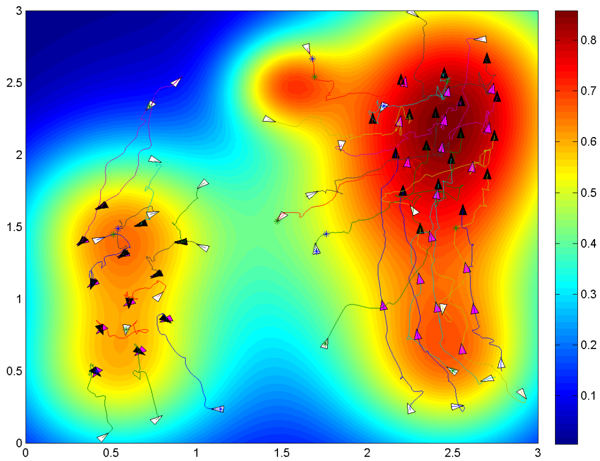

(a)

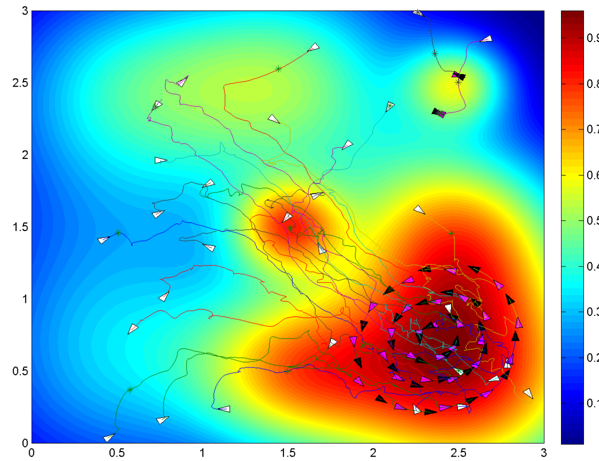

(b)

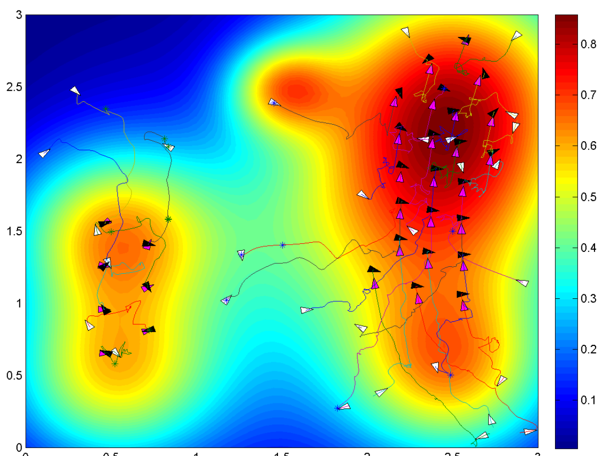

(c)

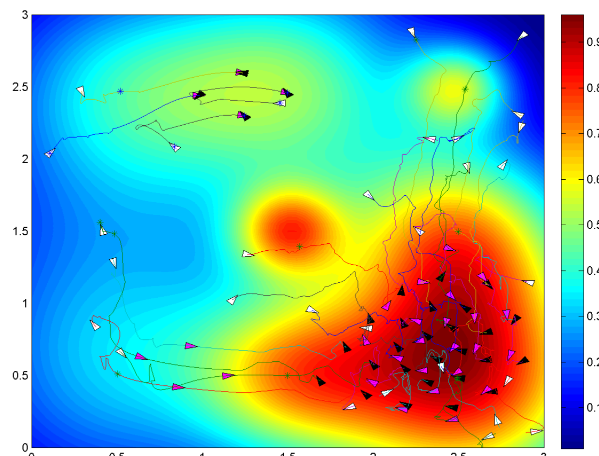

(d)

Figure 9: Trajectories of agents with the distributed adaptive control based on the gradient-based estimator with random initial values for $\hat{\theta}_i(0)$. (a) initial pose 1 and field 1, (b) initial pose 1 and field 2, (c) initial pose 2 and field 1, (d) initial pose 2 and field 2. The same notations are used as in Fig. 3(a).

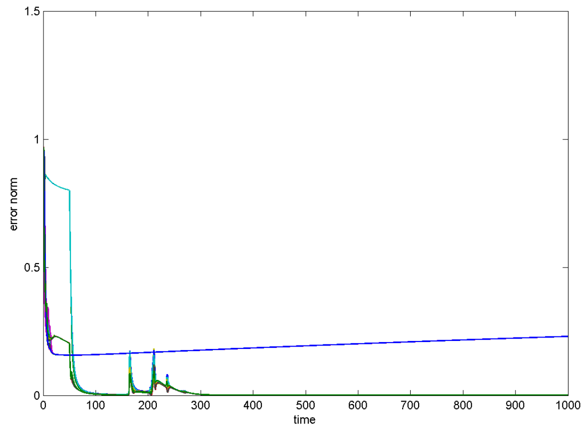

(a)

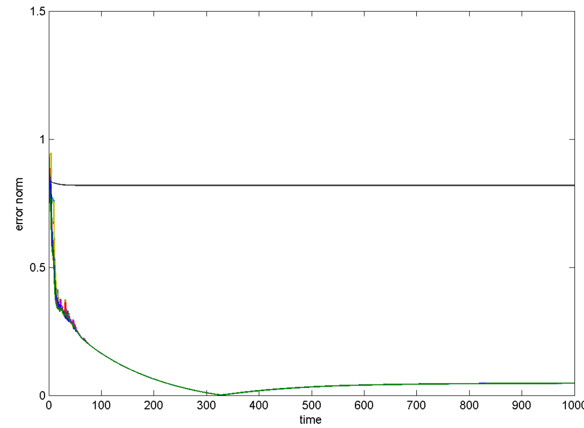

(b)

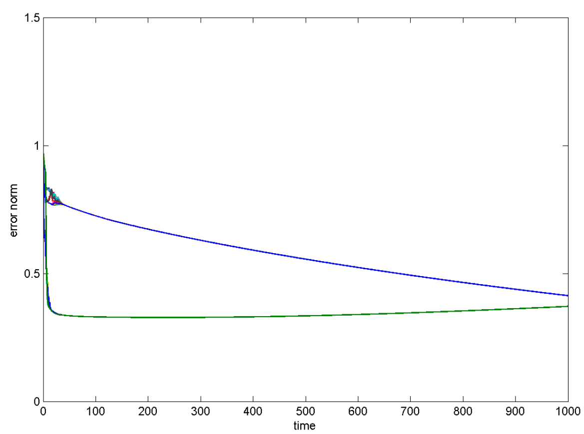

(c)

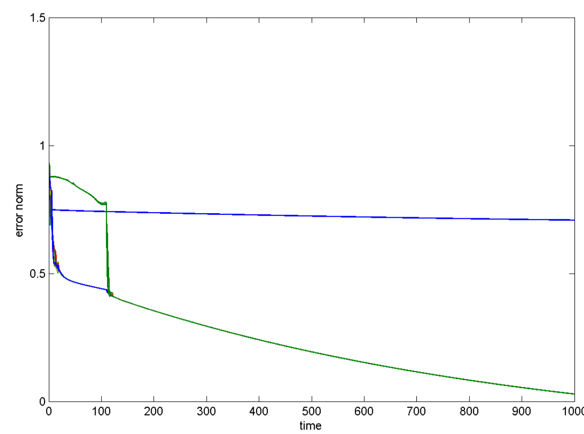

(d)

Figure 10: The norm of parameter estimation error, i.e., $\{\|\tilde{\theta}_i(t)\|\}$ by each agent with the distributed adaptive control based on the gradient-based estimator and random initial values for $\hat{\theta}_i(0)$ v.s. time. (a) initial pose 1 and field 1, (b) initial pose 1 and field 2, (c) initial pose 2 and field 1, (d) initial pose 2 and field 2.

differentially driven mobile robots, no sensor noise and a simple communication model (r-disk). Therefore, the future work is to extend the proposed approach in more realistic conditions and develop the stochastic version of this problem, taking into account the measurement sensor noise. Another future direction is to apply the proposed coordination algorithms to a group of robotic boats, which are being developed by the Professor Choi's group at Michigan State University.

Acknowledgment

This work has been supported, in part, by the National Science Foundation through CAREER Award CMMI-0846547. This support is gratefully acknowledged.

We appreciate valuable comments and suggestions of anonymous reviewers on improving the quality of the paper.

References

[1] M. M. Zavlanos and G. J. Pappas, "Potential fields for maintaining connectivity of mobile networks," *IEEE Transactions on robotics*, vol. 23, no. 4, 2007.

[2] Olfati-Saber, "Flocking for multi-agent dynamic systems: Algorithm and theory," *IEEE Transactions on Automatic Control*, vol. 51, no. 3, pp. 401–420, March 2006.

[3] W. Ren and R. W. Beard, "Consensus seeking in multiagent systems under dynamically changing interaction topologies," *IEEE Transactions on Automatic Control*, vol. 50, no. 5, pp. 655–661, May 2005.

[4] M. Schwager, D. Rus, and J. J. Slotine, "Decentralized, adaptive coverage control for networked robots," *International Journal of Robotics Research*, vol. 28, no. 3, pp. 357–375, March 2009.

[5] H. G. Tanner, A. Jadbabaie, and G. J. Pappas, "Stability of flocking motion," University of Pennsylvania, Technical Report, 2003.

[6] C. W. Reynolds, “Flocks, herds and schools: A distributed behavioral model.” *Computer Graphics*, vol. 21, no. 4, pp. 25–34, 1987.

[7] R. C. Eberhart, Y. Shi, and J. Kennedy, *Swarm Intelligence*, ser. The Morgan Kaufmann Series in Artificial Intelligence. Academic Press, 2001.

[8] E. Bonabeau, M. Dorigo, and G. Theraulaz, *Swarm Intelligence: From Natural to Artificial Systems*, ser. Santa Fe Institute Studies on the Sciences of Complexity. Oxford University Press, 1999.

[9] J. Choi, S. Oh, and R. Horowitz, “Distributed learning and cooperative control for multi-agent systems,” *Automatica*, vol. 45, no. 12, pp. 2802–2814, 2009.

[10] P. Ő gren, E. Fiorelli, and N. E. Leonard, “Cooperative control of mobile sensor networks: Adaptive gradient climing in a distributed envrironment,” *IEEE Transaction on Automatic Control*, vol. 49, no. 8, p. 1292, August 2004.

[11] N. Leonard, D. Paley, F. Lekien, R. Sepulchre, D. Fratantoni, and R. Davis, “Collective motion, sensor networks, and ocean sampling,” *Proceedings of the IEEE*, vol. 95, 2007.

[12] R. Bachmayer and N. E. Leonard, “Vehicle networks for gradient descent in a sampled environmen,” *in Proc. 41st IEEE Conf. Decision Control*, vol. 113 117, p. 113 117, 2002.

[13] J. Lawton, R. Beard, and B. Young, “A decentralized approach to formation maneuvers,” *IEEE Transactions on Robotics and Automation*, vol. 19, no. 6, pp. 933–941, 2003.

[14] W. Ren, “Consensus strategies for cooperative control of vehicle formations,” *Control Theory & Applications, IET*, vol. 1, no. 2, pp. 505–512, 2007.

[15] H. K. Khalil, *Nonlinear systems*. Prentice hall New Jersey, 2002.

[16] S. Sastry, *Nonlinear Systems Analysis, Stability, and Control*. Springer-Verlag, 1999.

[17] Y. Liu, Y. Jia, and N. Xi, "Dynamic model and adaptive tracking controller for 4-powered caster vehicle," in *2010 IEEE International Conference on Robotics and Automation (ICRA)*. IEEE, pp. 4940–4945.

[18] C. Godsil and G. Royle, *Algebraic Graph Theory*, ser. Graduate Text in Mathmatics. Springer-Verlag, 2001, vol. 207.